Interleaving Carbon-Glass veil in glass epoxy composite for improved mode-I fracture toughness– A hybrid approach

Vinayak S. Uppin, P. S. Shivakumar Gouda*, I. Sridhar, Aravind Muddebihal
Research Center, Department of Mechanical Engineering, SDM College of Engineering & Technology, Dharwad, Visvesvaraya Technological University, Belagavi, Karnataka, India.
ursuppin@gmail.com, ursshivu@gmail.com, sridhari74@gmail.com, aravindbm21@gmail.com

M. A. Umarfarooq
Center of Excellence in Material Science, School of Mechanical Engineering, KLE Technological University, India.
umarfarooq.ma@gmail.com

Abhilash Edacherian
Department of Mechanical Engineering, College of Engineering, King Khalid University, Abha, Saudi Arabia
edalheriad@kku.edu.sa

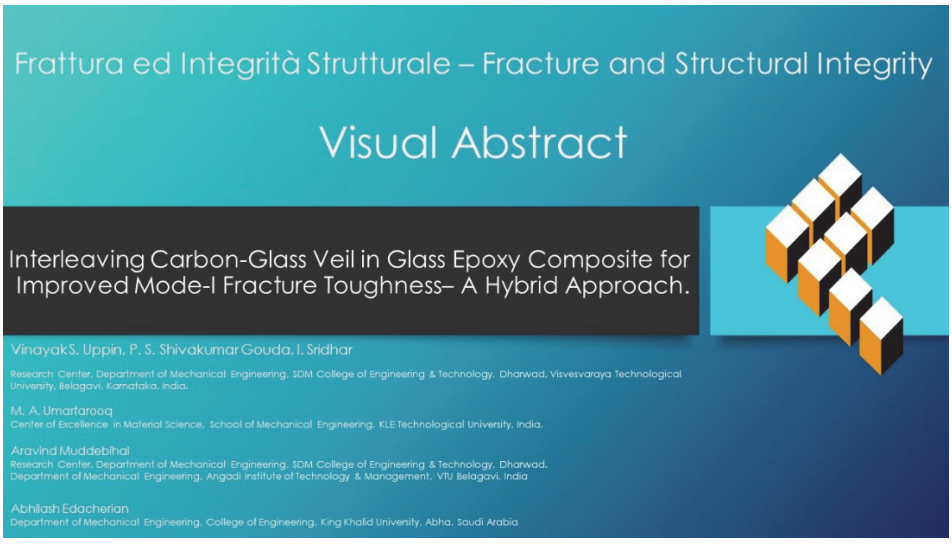

Citation: Uppin, V. S., Shvakumar Gouda, P.S., Sridhar I., Muddebihal, A., Umarfarooq, M.A., Edacherian, A., Interleaving carbon-glass veil in glass epoxy composite for improved mode-I fracture toughness– A hybrid approach, Frattura ed Integrità Strutturale, 68 (2024) 127-139.

Received: 24.11.2023
Accepted: 13.01.2024
Published: 24.01.2024
Issue: 01.04.2024

KEYWORDS. Hybrid Veil, Interlaminar fracture Toughness, Glass veil, Carbon veil, Fractography.

INTRODUCTION

Fiber-reinforced polymer composites offer a widespread range of applications in aerospace, automotive, defence, marine, and civil engineering due to their high specific strength and modulus, making them especially useful in constructing lightweight structures [1]. Despite of impressive in-plane properties of composite laminates, they are suspected of interlayer failure under typical operational environments. Many approaches have been followed to improve the IFT, including z-pins [2, 3], 3D fabrics [4,5], resin modification [6,7,8], modification of fiber surfaces [9,10], intra-reinforcement [11], and interleaving [12,13,14]. Inserting a thin nonwoven layer between the plies is known as the interleaving technique, which is the most prevalent approach to enhance the IFT due to its ease of manufacturing [15]. Moreover, interleaving of veils is scattered in a wide range, such as nano veils [13], micro veils [15-18], metal coated veils [19], electrospun veils [14,20], and hybrid veils [15,21-25]. Indeed, the hybrid veils interleaving approach is more promising for enhancing interlaminar fracture toughness. Quan et al. [16] demonstrated interleaving of hybrid thermoplastic veils (inter-ply of Polyphenylene sulphide and Polyamide12 veils at midplane) improves mode-I and mode-II fracture toughness in noncrimp carbon fiber (NCF) laminates by 273% and 206%, respectively. Kuwata et al. [18] reported that hybrid veil in polyester/carbon (70:30) showed more stable and improved fracture toughness when compared to carbon veil interleaved uni-directional CFRP composites. Quan et al. [25] demonstrated that interleaving veils produced by commingling of recycled carbon fibers (rCF) and Polyphenylene-sulfide (PPS) fibers have increased G_{IC} and G_{IP} by 195% and 220%, respectively, and in mode-II average IFT increased by 103%. Wong et al. [26] showed that the dissolving characteristics of phenoxy fiber hybrid interleaf (aramid and phenoxy fiber) in epoxy improve the interlaminar properties of carbon fiber-reinforced plastic (CFRP) laminates. Besides, multi-scale hybrid toughening mechanisms have shown a more promising strategy to improve the IFT [27]. Eskizeybek et al. [21] observed a 77% increase in mode-I energy release rate for CFRP composites interleaved with carbon nanotubes (CNTs) reinforced polyacrylonitrile (PAN) electro-spun hybrid mats. Chen et al. [28] developed multi-toughened veils interleaved in CFRP laminates. The veil comprised of nano-scale core-shell rubber (CSR) and micro-scale short carbon fiber (SCF). The mode-I and Mode-II critical energy release rates were improved by 127% and 154% for multi-scale toughened CFRP composites, without compromising the mechanical properties and glass transition temperature. In another work [15], the mode-I fracture toughness of a hybrid veil interleaved composite (20 g/m^2 carbon veil + 10% CSR nanoparticles) was increased by 218% and 217% during initiation and propagation, respectively. In most of the hybrid veils interleaved composites, a multi-scale toughening mechanism such as extrinsic and intrinsic toughening was reported, but the processing of these veils is quite difficult compared to microfiber veil interleaving [27]. Furthermore, the type of base reinforcement, fiber dispersion, fiber length, binders used to form veils, and the areal density of interleaving materials have a substantial influence on interlaminar fracture toughness [29-34]. Beylergil et al. [30] conducted a study to examine the impact of different areal densities (17 and 50 g/m^2) of polyamide-66 (PA 66) nonwoven veils on fracture toughness. Their findings revealed a significant enhancement in IFT, $G_{IC,}$ and G_{IP} of 349% and 718% respectively. Wang et al. [34] reported that the binder used to form carbon veils has a noticeable effect on fracture energy, crack path, and R-curve behavior compared to polyphenylene sulfide veils. Beckerman et al. [35] developed unidirectional Carbon epoxy composite laminates by interleaving PA66 veils of various areal densities (1.5 g/m^2, 4.5 g/m^2, and 9 g/m^2). The fracture toughness of 4.5 g/m^2 PA66 veil interleaved sample shows an improvement of about 156% and 69% under Mode I and Mode II loadings respectively. Moreover, enhancing IFT relied on energy dissipation, quantitative fiber bridging, and deflection of the crack path along the path was closely related to fiber and matrix distribution around the delamination front [36].

Nevertheless, there has been limited research on the impact of micro-fiber hybridization was reported. This research addresses this gap by exploring the impact of interleaving material hybridization in Glass epoxy composites using two novel approaches, namely, inter-ply veil and inter-weaved veil. Further, a mode-I fracture study was conducted to know the influence of interleaving approaches on interlaminar fracture toughness. Additionally, Scanning Electron Microscopy (SEM) is employed to examine fracture samples and elucidate the underlying fracture mechanisms. The subsequent sections provide comprehensive information on the materials used, the hybrid veil weaving process, laminate preparation, and test procedure.

EXPERIMENTAL

Materials

Uni-Directional (UD) glass fabric used in this study was supplied by Mark-Tech Private Limited, Bangalore, India with an areal density of 220 g/m^2. To manufacture laminates, a two-part epoxy resin (Araldite LY 556 epoxy and HY 951 hardener) was sourced from Zenith Industrial Suppliers, Bangalore, India. Mechanical and physical properties of the fiber and resin are listed in Tab. 1. The glass and carbon interleaving veils were supplied by Essen

International, India. Nonwoven glass veil of 30 GSM (Grams per Square Meter) has a diameter of 11 microns, while the carbon veils (15, 20, and 30 GSM) have a diameter of 7 microns and approximate lengths of 6 and 12 mm.

Constituents	Density (kg/m³)	Tensile Strength (MPa)	Young's Modulus (GPa)	Failure strain (%)
Fiber	2600	2000	78	4.8
Resin	1140	73.3	3.4	4.5

Table 1: Physical and Mechanical Properties of Fiber and Matrix.

Weaving of nonwoven Glass and Carbon veil

The hybrid glass carbon veil was produced by the plain weaving technique. Initially, the glass and carbon veils were stripped with 5 mm width. The strips were arranged in a plain-woven pattern [37], with each filling strip alternating over and under each warp yarn, ensuring a high number of intersections. Special attention was given to minimizing gaps between the glass and carbon strips. The weaving process for interweaved non-woven veils is illustrated in Fig. 1. The same technique was followed to produce other interweaved veils, by varying the areal density of non-woven carbon veils. The details about sample code and description of different hybrid veil interleaved are mentioned in Tab. 2.

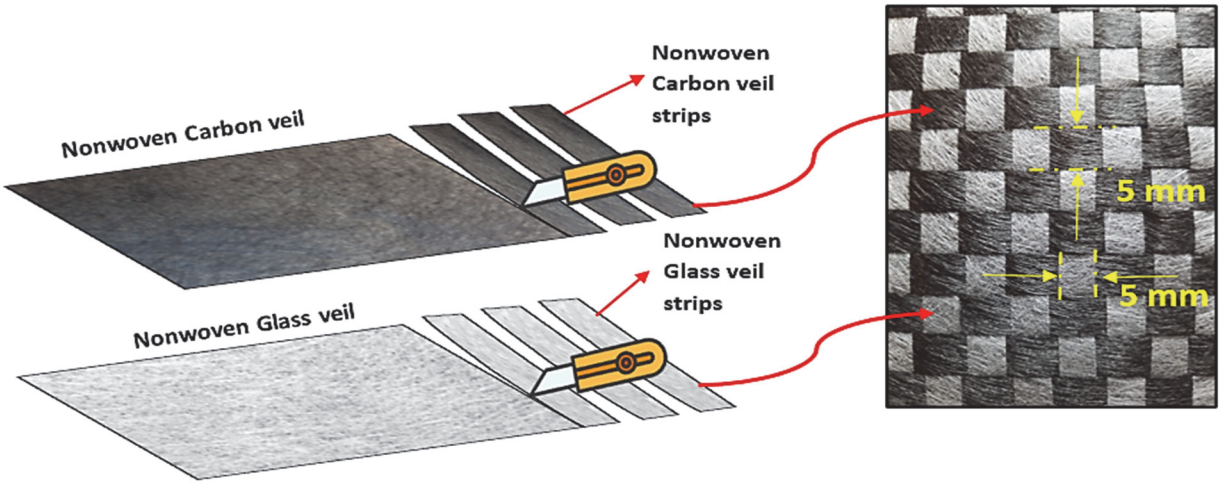

Figure 1: Schematic diagram showing the preparation of weaved Glass-Carbon veil.

Sl. No	Code	Inter ply Glass-Carbon ply	Inter-weaved Glass-Carbon ply	Description
1	Plain	X	X	Non-interleaved Glass epoxy composite
2	I-C15G30	√	X	Inter-ply interleaved - 15GSM Carbon and 30 GSM Glass
3	I-C20G30	√	X	Inter-ply interleaved - 20GSM Carbon and 30 GSM Glass
4	I-C30G30	√	X	Inter-ply interleaved - 30GSM Carbon and 30 GSM Glass veil
5	W-C15G30	X	√	Inter-weaved interleaved – Strips of 15GSM Carbon and 30 GSM Glass veil
6	W-C20G30	X	√	Inter-weaved interleaved - Strips of 20GSM Carbon and 30 GSM Glass veil
7	W-C30G30	X	√	Inter-weaved interleaved - Strips of 30GSM Carbon and 30 GSM Glass veil

Table 2: Composite Laminates code and their details.

Laminate manufacturing

Sixteen layers of glass fabrics with a size of 300 x 210 mm (width x breadth) were manually stacked on a flat mould (steel plate coated with mould release agent) to produce with and without interleaved composite laminates, as shown in Fig. 2. To produce an initial interlaminar crack in the specimens, a thin Teflon film of 14 μm was placed at the mid-plane between the 8th and 9th layer, as shown in Fig. 2(a). Glass and Carbon veils were used as interlayer toughening materials by adopting two approaches (a) inter-ply veils and (b) inter-weaved veils. In inter-ply veils approach, one layer of Glass veil (30 GSM) and one layer of Carbon veil (15, 20, 30 GSM) were placed at the mid-plane of laminate. Fig. 2(b) illustrates a schematic illustration of the inter-ply veil stacking procedure. In inter-woven veil approach, the plain interweaved veil was placed in between 8th and 9 the layer as illustrated in Fig. 2(c). Besides, the stacked laminates were cured at room temperature for an about 24 hours and then specimens were cut as per the dimensions prescribed in ASTM D5528 [38].

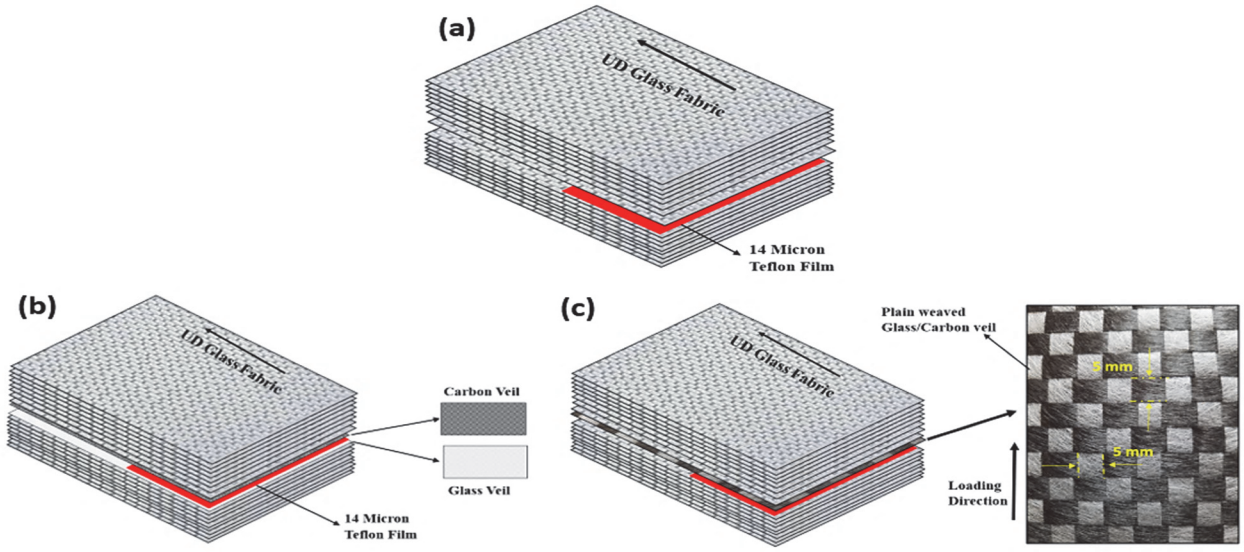

Figure 2: Stacking Sequence of Hybrid veils in laminate, (a) Plain (b) Inter-ply interleaved, and (c) Inter-weaved ply Interleaved

Mode-I Fracture Test

DCB samples were prepared for mode-I IFT test in accordance with ASTM D5528 [38]. Specimen size of 150×20mm (length×width) were cut from base laminate and piano hinges were bonded on outer faces above and below the pre-crack which is shown in Fig. 3. DCB cross-section along the lengthwise were sprayed with water-based white paint. For every 1 mm, a line was marked on the white paint for better visualization of crack growth. To capture the crack growth, a video camera with a resolution of ±0.5mm was employed. Each sample was loaded in a Universal testing machine (UTM) with a displacement rate of 2 mm/min and load-displacement values were recorded as per the ASTM procedure. For each composition, five samples were tested. The mode-I IFT was calculated using the modified beam theory (MBT) Eqn. (1).

$$G_I = \frac{3P\delta}{2B\left(a+|\Delta|\right)} \tag{1}$$

where, 'P', 'δ', 'B', 'a', and 'Δ' represent the load, displacement, width, crack length, and correction factor respectively and Δ is an effective delamination extension to correct for the rotation of DCB arms at the delamination front. Which is determined experimentally by generating a least square plot of the cube root of compliance ($C^{1/3}$) as a function of delamination length.

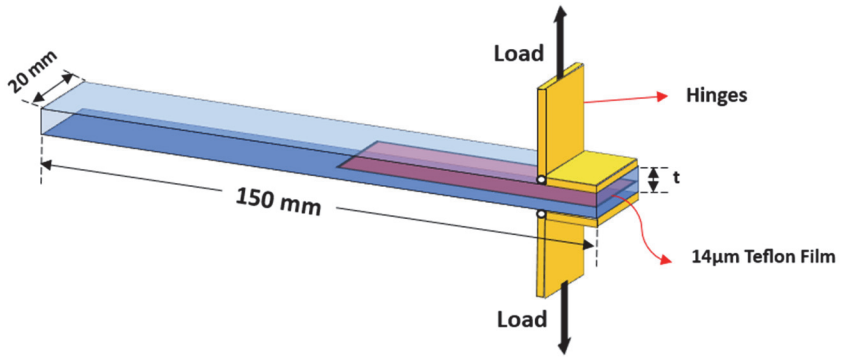

Figure 3: Dimensions and position of piano hinges and pre-crack in DCB sample

RESULTS AND DISCUSSION

Mode-I Fracture test

Fig. 4 depicts the load-displacement curves of DCB specimens under Mode-I loading. The maximum load taken by DCB samples are of 28N, 29N, 26N, 34N, 32N, 31N, and 33N for plain, I-C15G30, I-C20G30, I-C30G30, W-C15G30, W-C20G30, and W-C30G30 respectively. For plain samples, a slightly jagged load-displacement curve was obtained, indicating unstable crack propagation and it is witnessed through earlier studies [30]. However, in case of veil-interleaved samples, a more stable crack propagation was observed which is seen in Fig. 4. Moreover, the magnitude of energy required to propagate per unit area of crack varied in all interleaved samples, which depends on the alignment of fibers around the delamination front, resin dispersion, and through-width variation of the crack front [25]. Based on the observations made during the DCB test, the fiber bridging and propagation path were not identical for inter-ply and inter-weaved veil interleaved samples.

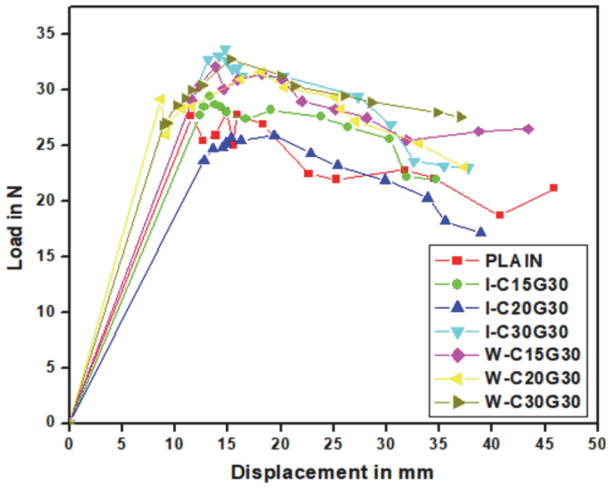

Figure 4: Load versus displacement of Mode-I test.

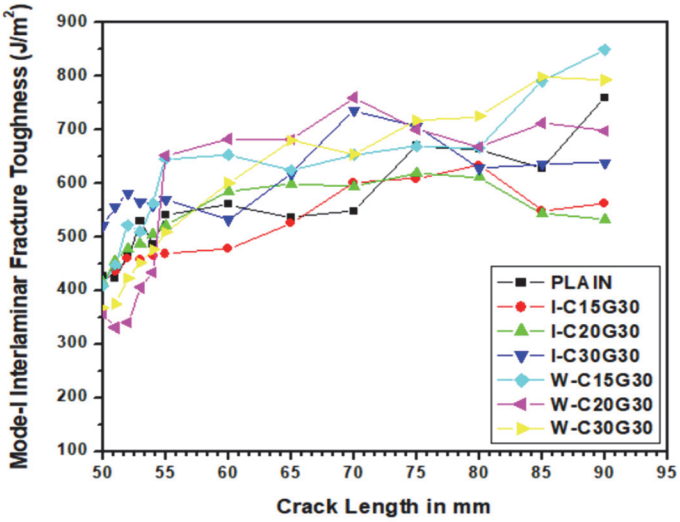

Figure 5: R-Curves for interleaved and non-interleaved composite laminates.

Fig. 5 displays the delamination resistance curves (R-curves) for all the interleaved and plain samples with reference to crack length. The machine-recorded time during mode-I test was compared with the recorded time video camera to select the load-displacement values, these values play a vital role in finding the interlaminar fracture toughness as per modified beam theory. The scattered R-curves trend indicates evidence of different failure mechanisms. Rising R-curves are a common characteristic of the test due to the increasing fiber bridging region behind the crack front during growth [17]. In inter-ply veil interleaved composite samples, the R-curves were increased as the areal density of the carbon veil increased. However, in the interweaved veil case, the effect of carbon veil areal density was negligible, indicating that the interleaving architecture has a significant effect on interlaminar fracture toughness. This can also be seen in IFT initiation and propagation values

which are depicted in Fig. 6. The summary of initiation fracture toughness of all the specimens is depicted in Fig. 6(a). Plain samples showed, a G_{IC} of 477±12.67 J/m². In comparison, the inter-ply veil interleaved samples, I-C15G30 and I-C20G30, exhibited G_{IC} values of 449±18.23 J/m² and 476±20.53 J/m² respectively, indicating a 5.87% and 0.2% decrease when compared to plain samples. This is due to poor bonding and rich resin resulting in decreased initial fracture toughness. Even Kuwata et al. [18] reported that the interleaving of two carbon veils (10 gsm each) at midplane showed a poor IFT. Remarkably, the I-C30G30 sample demonstrated a G_{IC} of 558±19.28 J/m², with a 16.98% improvement over the plain sample. In contrast, the inter-weaved veil configuration namely, W-C15G30 sample showed a G_{IC} of 515±18.73 J/m², indicating a 7.96% increase, while further increasing carbon veil areal density in W-C20G30 and W-C30G30 samples resulted in G_{IC} values of 419±15.12 J/m² and 433±19.73 J/m² which is 12.15% and 9.22% less than the plain sample respectively. Fig. 6(b) represents the IFT of propagation as a summary of all specimens. The Plain sample exhibited a G_{IP} of 622±20.34 J/m². However, the I-C15G30 and I-C20G30 samples showed G_{IP} values of 565±23.18 J/m² and 583±21.17 J/m², respectively, indicating 9.16% and 6.27% decreases compared to the plain sample. This reduction in G_{IP} was attributed to poor fiber bridging and it is depicted in Fig. 7(b) and (c). Conversely, the I-C30G30 sample displayed a G_{IP} of 641±17.93 J/m², with a 3.05% improvement over the plain sample. This is due to carbon fiber pulled-out and moderate fiber bridging shown in Fig. 7(d). In case of inter-weaved veil samples, the G_{IP} values for W-C15G30, W-C20G30, and W-C30G30 were 700±20.43 J/m², 699±19.17 J/m², and 708±20.53 J/m² with 12.54%, 12.37%, and 13.82% higher than that of plane samples respectively. The rich fiber bridging, crack migration, and fiber pullout helped to improve the fracture toughness during propagation shown in Figs. 7 (e), (f), and (g). The percentage of variation in IFT during initiation and propagation corresponding to the plain sample is also listed in Tab. 3.

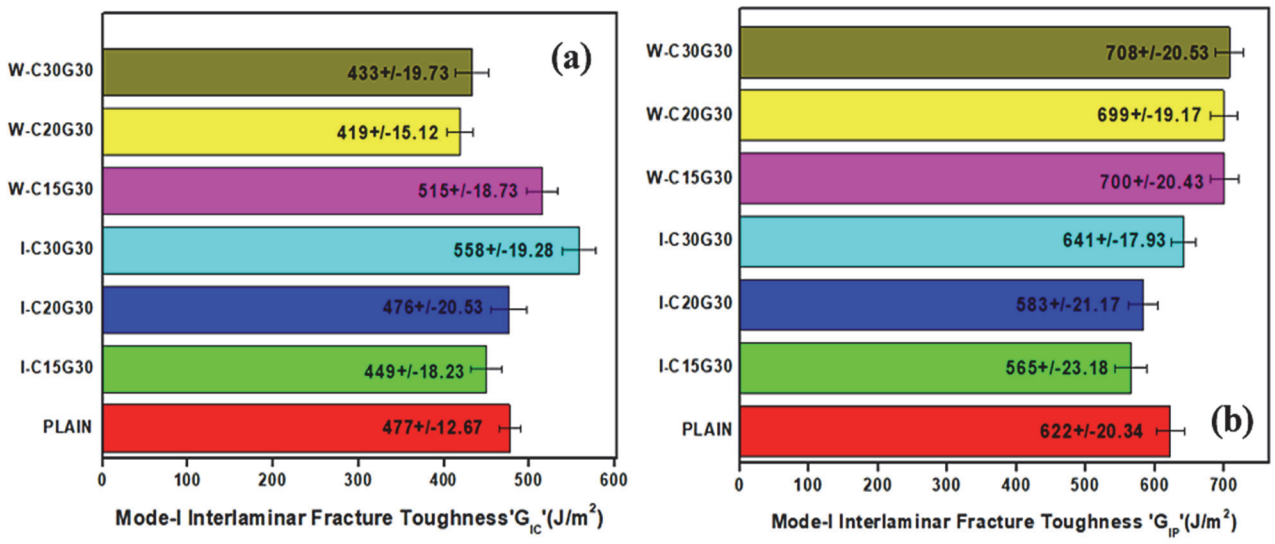

Figure 6: Mode-I IFT (a) Initiation (GIC) (b) Propagation (GIP)

Sample Code	G_{IC}(J/m²)	Variation (%)	G_{IP}(J/m²)	Variation (%)
Plain	477	--	622	--
I-C15G30	449	-5.87	565	-9.16
I-C20G30	476	-0.20	583	-6.27
I-C3030	558	+16.98	641	+3.05
W-C15G30	515	+7.96	700	+12.54
W-C20G30	419	-12.15	699	+12.37
W-C30G30	433	-9.22	708	+13.82

Table 3: Variation of initiation and Propagation IFT.

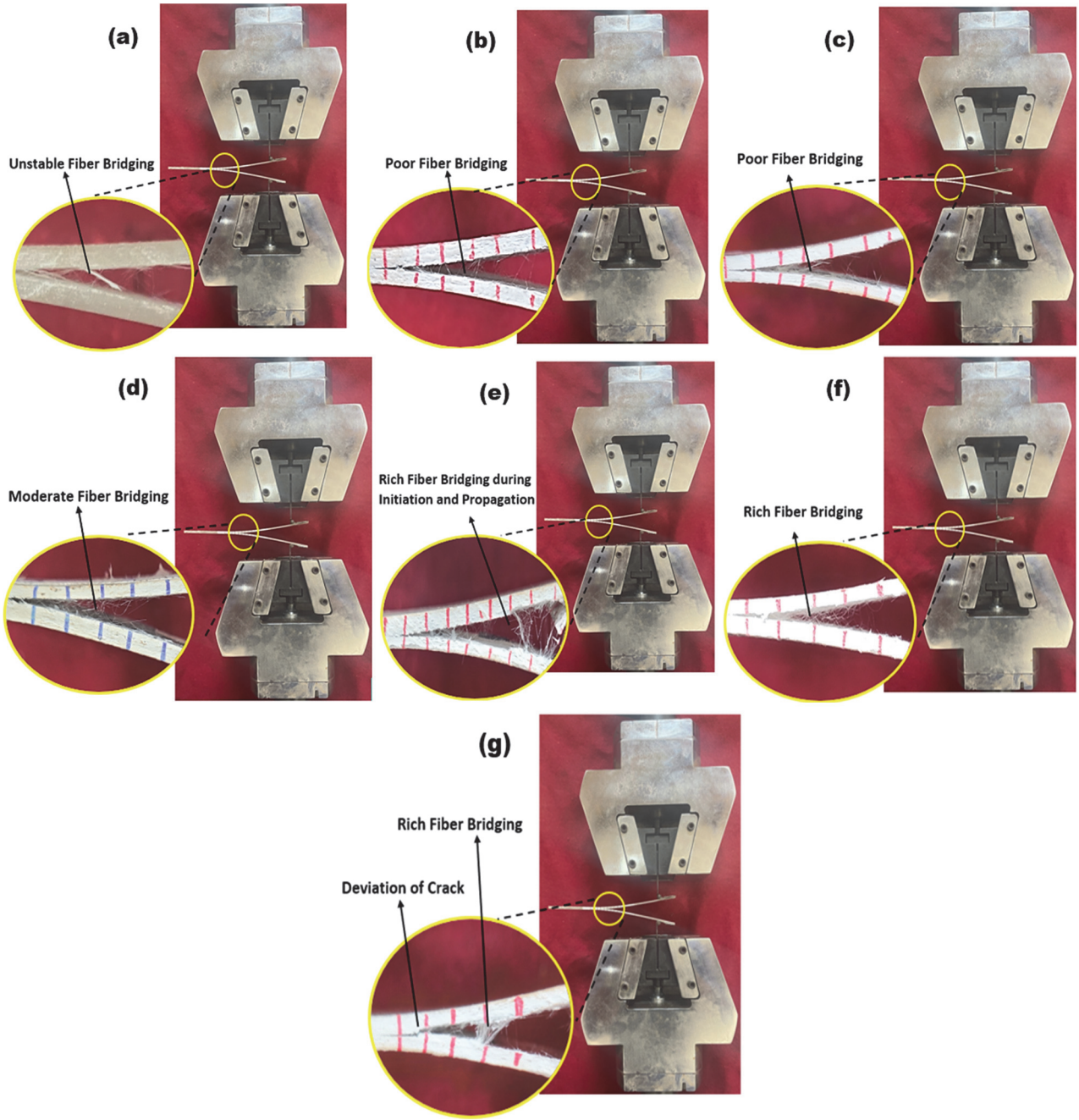

Figure 7: Fiber Bridging under Mode-I test (a) Plain (b) I-C15G30 (c) I-C20G30 (d) I-C30G30 (e) W-C15G30 (f) W-C20G30 and (g) W-C30G30

A pair of fractured surfaces for inter-ply and weaved veil interleaved composites are shown in Fig. 8. The fractured surfaces of I-C15G30 and I-C20G30 samples showed a tiny rough surface which is associated with a poor interface between the glass and carbon veils (Fig. 8 (a) and (b)). In micrographs of I-C15G30 specimen, a fiber fracture, minor fiber imprints, and epoxy tend to separate from the fiber surface were observed in Fig. 9 (a) and (b), which indicates the crack was more predominantly propagated through the glass veil. Besides, in micrographs of I-C20G30 specimen the rich fiber imprints on both faces of the fractured interface and rich resin zone were observed in Fig. (9) (c) and (d), this represents the poor bonding between fiber and epoxy with the absence of plastic deformation. Surprisingly in I-C30G30, the crack is predominantly grown through the veil interface and marginal carbon fibers pulled out during crack initiation and propagation were noticed in Fig. 8 (c). The micrographs of I-C30G30 are shown in Fig. 9 (e) and (f), indicating rich fiber imprints and fibers were covered with a layer of epoxy and it peeled out from the fiber surface during crack propagation and a formation of veil fiber residue is also present, this morphology represents the crack followed a tortuous path.

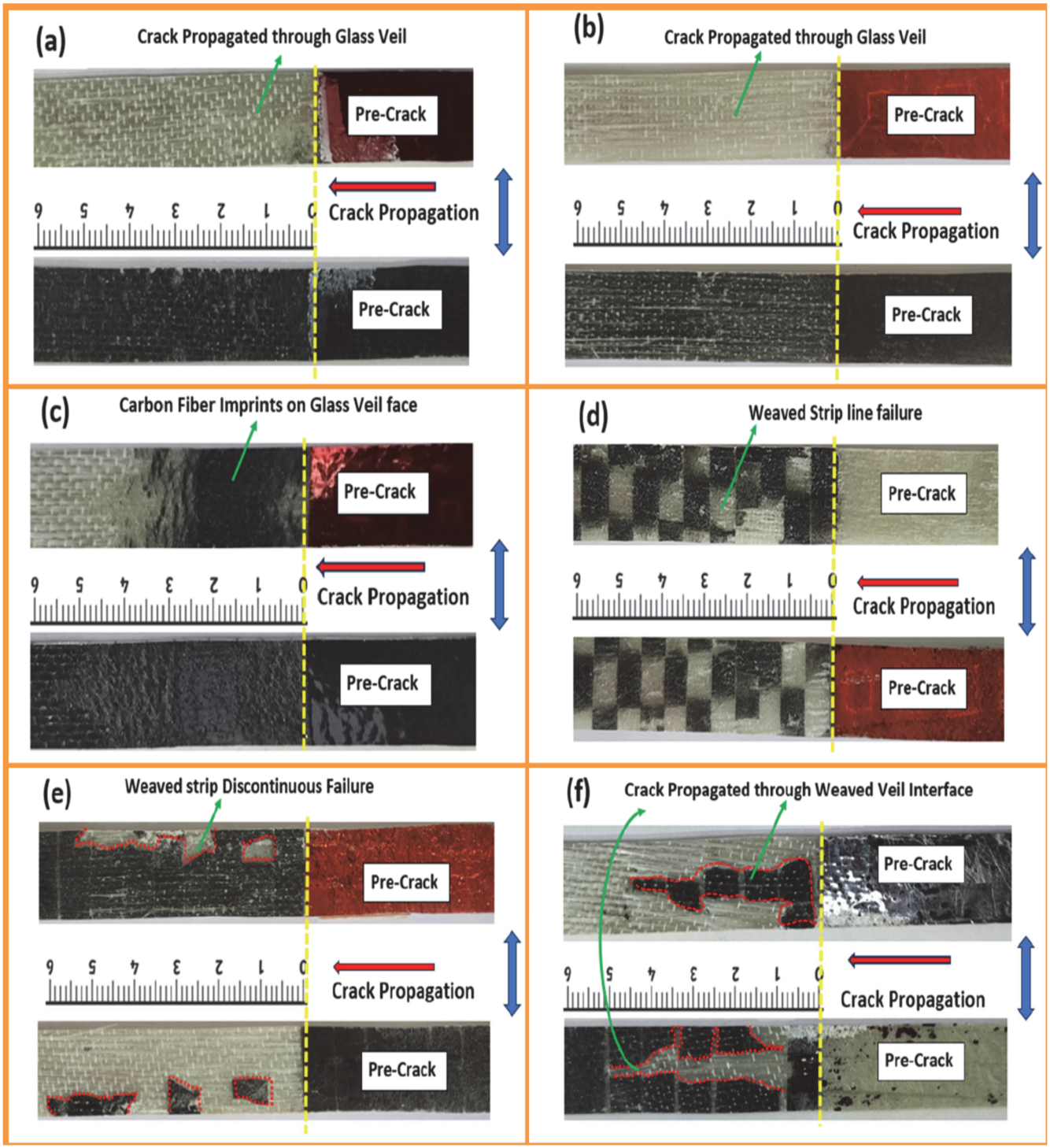

Figure 8: Interface of fractured DCB samples (a) I-C15G30 (b) I-C20G30 (c) I-C30G30 (d) W-C15G30 (e) W-C20G30 and (f) W-C30G30

Furthermore, in W-C15G30 the crack propagated through the veil interface seen in Fig. 8 (d) in which the plain weaved architecture at the interface helps to migrate the crack and encounter more resistance during initiation and propagation. Photomicrographs in Fig. 9 (g) and (h) show that the fibers were covered with epoxy and residue of veil fibers, and a deformed matrix, which indicates more energy absorption while propagating crack. In W-C20G30 and W-C30G30 specimens, the crack propagated majorly through the neighbor side (glass veil) and with rich resin pockets in the glass veil which restricted attaining higher IFT during initiation. But, during propagation, the carbon fibers pulled out from weaved strips were observed which is represented in Fig. 8 (e) and (f). The photomicrographs of W-C20G30 indicate the fractured

fibers and segmental debonding of fibers from the matrix in Fig. 9 (i) and (j). But in W-C30G30 the fractured fibers, embedded fibers in epoxy, and epoxy deformation was observed in Fig. 9 (k) and (l). The fiber bridging and crack path migration helped to achieve rich extrinsic toughening.

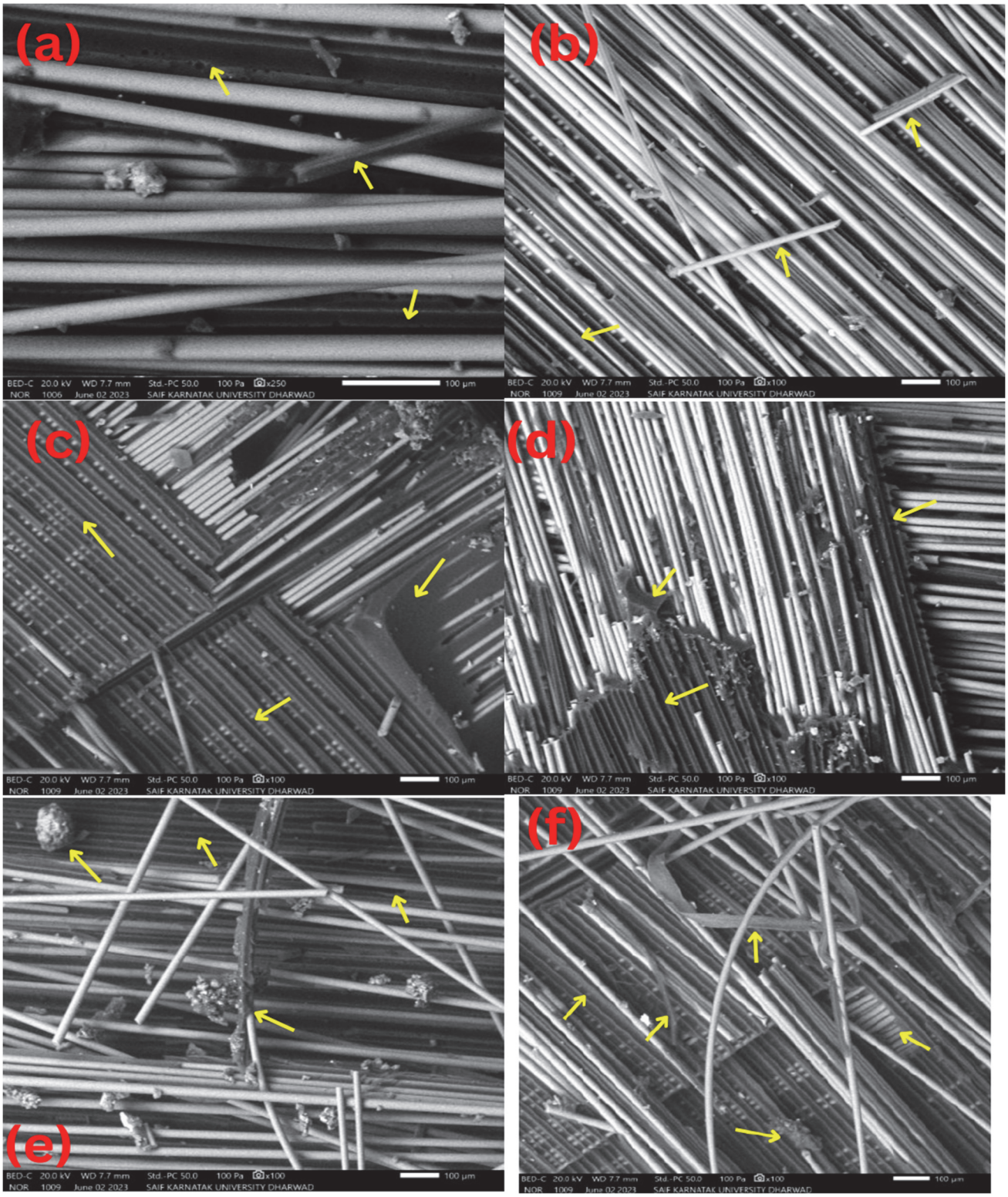

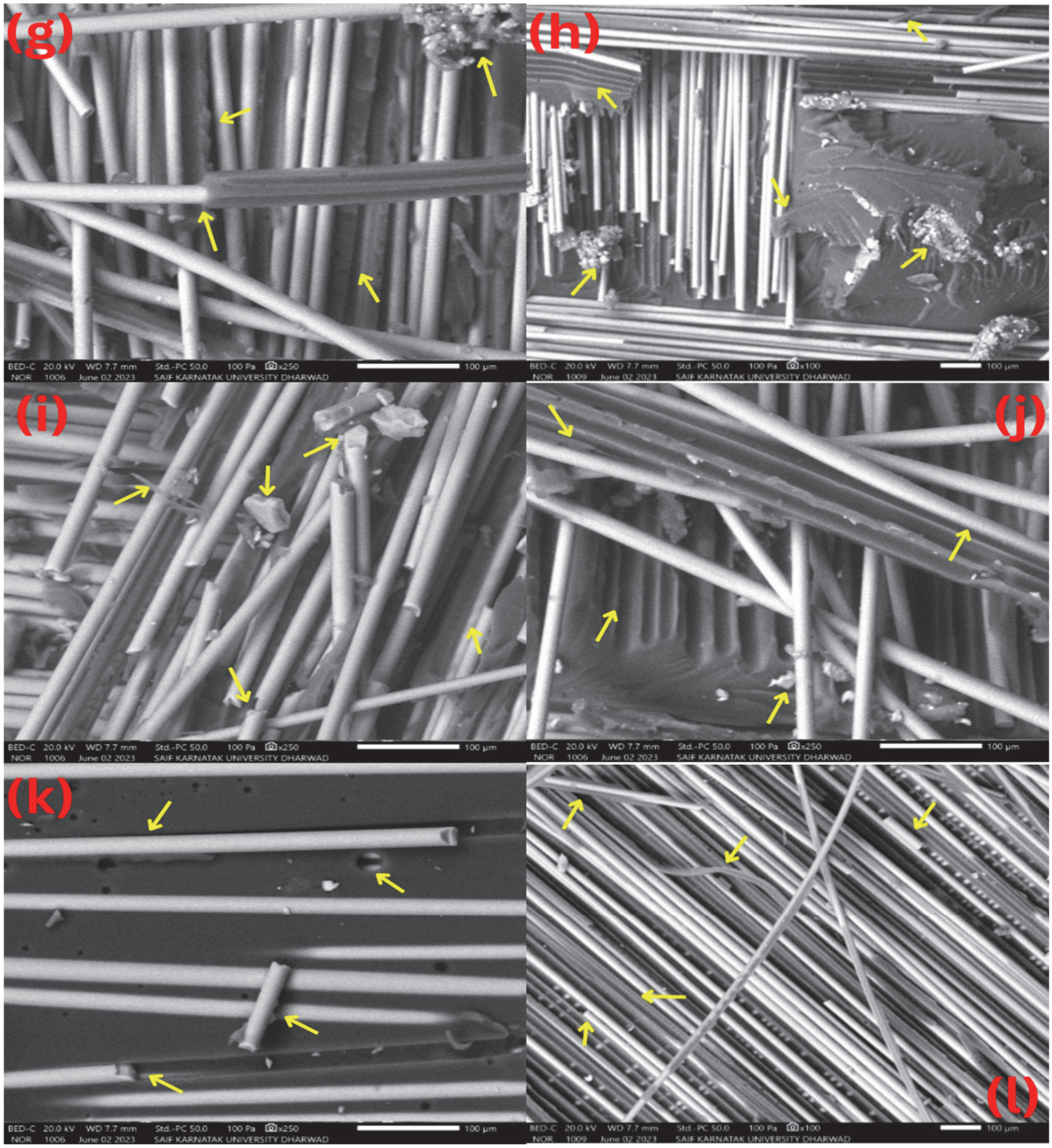

Figure 9: SEM images of opening mode failure samples (a) I-C15G30-Upperside (b) I-C15G30-lower side(c)I-C20G30-Upperside (d)I-C20G30-lower side (e) I-C30G30-Upperside (f) I-C30G30-lower side(g)W-C15G30-Upperside(h)W-C15G30-lower side(i)W-C20G30-Upperside(j)W-C20G30-lower side (k) W-C30G30-Upperside and (l) W-C30G30-lower side

Conclusions

In summary, the plain inter-weaved veil using glass and carbon veil strips was developed and two approaches of interleaving such as inter-ply and plain inter-weaved veils were successfully demonstrated. In case of inter-ply veil interleaving approach, the improved fracture toughness (G_{IC} and G_{IP}) of about 17% and 3% was observed for I-

C30G30 sample. On the other hand, I-C15G30, and I-C20G30 samples exhibited a lower performance during both initiation and propagation when compared to plain sample. In case of inter-weaved veil approach, an improved fracture toughness (G_{IC} and G_{IP}) of about 8% and 13% was observed for W-C15G30 sample, but W-C20G30 and W-C30G30 showed a reduced fracture toughness (G_{IC}) of about 12% and 10% and an improved fracture toughness (G_{IP}) of about 13% and 14% respectively when compared to the plain sample. The main toughening mechanisms such as fiber bridging, crack deflection, fiber pull out, and epoxy deformation contributed to improving fracture toughness. Consequently, the insight gained from this work is interleaving veil architecture plays a predominant role in improving the interlaminar properties of glass epoxy composites.

ACKNOWLEDGMENT

The authors are pleased to convey their gratitude to the organization for providing the necessary amenities at the Research Centre, Mechanical Engineering and Geology Department of SDM College of Engineering and Technology, Dharwad.

FUNDING

The authors extend their appreciation to the Deanship of Scientific Research at King Khalid University for funding this work through the large group Research Project under grant number RGP2/415/44.

REFERENCES

[1] Chawla, K., Ray-Chaudhuri, S., Kitey, R. (2019). Interlaminar Fracture Toughness of Short Fibre Reinforced GFRP Laminates, Procedia Structural Integrity, 14, pp. 571–576. DOI: 10.1016/j.prostr.2019.05.070.

[2] Partridge, I.K., Cartié, D. (2005). Delamination resistant laminates by Z-Fiber® pinning: Part I manufacture and fracture performance, Composites Part A: Applied Science and Manufacturing, 36(1), pp. 55–64. DOI 10.1016/j.compositesa.2004.06.029.

[3] F. Pegorin., K. Pingkarawat., Mouritz, A.P. (2015). Comparative study of the mode I and mode II delamination fatigue properties of z-pinned aircraft composites, Materials in Engineering, 65, pp. 139–146. DOI: 10.1016/j.matdes.2014.08.072.

[4] Fishpool, D.T., Rezai, A., Baker, D., Ogin, S.L., Smith, P.A. (2013). Interlaminar toughness characterisation of 3D woven carbon fibre composites, Plastics, Rubber and Composites, 42(3), pp. 108–114. DOI: 10.1179/1743289812y.0000000036.

[5] Sun, R., Li, Z., Guo, L., Yu, H., Zhang, L., Zong, Q. (2022). A mesoscale in situ method for assessing fracture toughness of intra-yarn and interface in 3D woven composites, Composites Science and Technology, 224, p. 109447. DOI: 10.1016/j.compscitech.2022.109447.

[6] Prasad, V., Sekar, K., Varghese, S., Joseph, M.A. (2019). Enhancing Mode I and Mode II interlaminar fracture toughness of flax fibre reinforced epoxy composites with nano TiO2, Composites Part A: Applied Science and Manufacturing, 124, p. 105505. DOI: 10.1016/j.compositesa.2019.105505.

[7] Shivakumar Gouda, P.S., Chatterjee, V., Barhai, P.K., Jawali, D., Rahatekar, S., Wisnom, M.R. (2014). Improved fracture toughness in carbon fibre epoxy composite through novel pre-preg coating method using Epoxy Terminated Butadiene Nitrile rubber, Materials and Design (1980-2015), 62, pp. 320–326. DOI: 10.1016/j.matdes.2014.05.018.

[8] Joshi, A., Gouda, S., Sridhar, I., Umar, A., Vinayak Uppin., B. H. Maruthi Prashanth. (2023). Matrix Hybridization Effects on Interlaminar Fracture Toughness of Glass Epoxy Laminates using Nano and Micro fillers, Fracture and Structural Integrity, 17(65), pp. 59–73. DOI: 10.3221/igf-esis.65.05.

[9] Wang, C., Ji, X., Roy, A., Silberschmidt, V.V., Chen, Z. (2015). Shear strength and fracture toughness of carbon fibre/epoxy interface: effect of surface treatment, Materials and Design, 85, pp. 800–807. DOI: 10.1016/j.matdes.2015.07.104.

[10] Martínez-Landeros, V.H., Vargas-Islas, S.Y., Cruz-González, C.E., Barrera, S., Mourtazov, K., Ramírez-Bon, R. (2019). Studies on the influence of surface treatment type, in the effectiveness of structural adhesive bonding, for carbon fiber reinforced composites, Journal of Manufacturing Processes, 39, pp. 160–166. DOI: 10.1016/j.jmapro.2019.02.014.

[11]Gouda, S., Joshi, A., I, S., M A, U., Uppin, V., Vastrad, J., Gogoi, N., Edacherian, A. (2022). Crack suppression by natural fiber integration for improved interlaminar fracture toughness in fiber hybrid composites, Frattura Ed Integrità Strutturale, 16(60), pp. 158–173. DOI: 10.3221/igf-esis.60.12.

[12] Quan, D., Deegan, B., R.C. Alderliesten., Clemens Dransfeld., Murphy, N., Alojz Ivanković., Rinze Benedictus. (2020). The influence of interlayer/epoxy adhesion on the mode-I and mode-II fracture response of carbon fibre/epoxy composites interleaved with thermoplastic veils, Materials and Design, 192, pp. 108781–108781. DOI: 10.1016/j.matdes.2020.108781.

[13] Ou, Y., González, C., Vilatela, J.J. (2020). Understanding interlaminar toughening of unidirectional CFRP laminates with carbon nanotube veils, Composites Part B: Engineering, 201, p. 108372. DOI: 10.1016/j.compositesb.2020.108372.

[14] Aljarrah, M.T., Abdelal, N.R. (2019). Improvement of the mode I interlaminar fracture toughness of carbon fiber composite reinforced with electrospun nylon nanofiber, Composites Part B: Engineering, 165, pp. 379–385. DOI: 10.1016/j.compositesb.2019.01.065.

[15] Wang, S., Mehmet Çağatay Akbolat., K.B. Katnam., Zou, Z., Potluri, P., Sprenger, S., Taylor, J. (2022). On the R-curve behaviour of carbon/epoxy laminates with core-shell rubber nanoparticle and micro-fibre veil hybrid toughening: Carbon vs PPS veils, Polymer, 254, pp. 125081–125081. DOI: 10.1016/j.polymer.2022.125081.

[16] Quan, D., Alderliesten, R., Dransfeld, C., Murphy, N., Ivanković, A., Benedictus, R. (2020). Enhancing the fracture toughness of carbon fibre/epoxy composites by interleaving hybrid meltable/non-meltable thermoplastic veils, Composite Structures, 252, p. 112699. DOI: 10.1016/j.compstruct.2020.112699.

[17] Vallack, N., Potluri, P., Sampson, W.W. (2023). Dependence on fibre type of interlaminar fracture toughness enhancement in interleaved polymer composites, Composites Science and Technology, 241, pp. 110135–110135. DOI: 10.1016/j.compscitech.2023.110135.

[18] Kuwata, M., Hogg, P.J. (2011). Interlaminar toughness of interleaved CFRP using non-woven veils: Part 1. Mode-I testing, Composites Part A: Applied Science and Manufacturing, 42(10), pp. 1551–1559. DOI: 10.1016/j.compositesa.2011.07.016.

[19] Liu, H., Guo, Y., Zhou, Y., Wan, G., Chen, Z., Jia, Y. (2021). Multifunctional nickel-coated carbon fiber veil for improving both fracture toughness and electrical performance of carbon fiber/epoxy composite laminates, Polymer Composites, 42(10), pp. 5335–5347. DOI: 10.1002/pc.26227.

[20] Beylergil, B., Tanoğlu, M., Aktaş, E. (2017). Enhancement of interlaminar fracture toughness of carbon fiber-epoxy composites using polyamide-6,6 electrospun nanofibers, Journal of Applied Polymer Science, 134(35), p. 45244. DOI: 10.1002/app.45244.

[21] Volkan Eskizeybek., Yar, A., Ahmet Avcı. (2018). CNT-PAN hybrid nanofibrous mat interleaved carbon/epoxy laminates with improved Mode I interlaminar fracture toughness, Composites Science and Technology, 157, pp. 30–39. DOI: 10.1016/j.compscitech.2018.01.021.

[22] Wang, J., Ma, C., Chen, G., Dai, P. (2020). Interlaminar fracture toughness and conductivity of carbon fiber/epoxy resin composite laminate modified by carbon black-loaded polypropylene non-woven fabric interleaves, Composite Structures, 234, p. 111649. DOI: 10.1016/j.compstruct.2019.111649.

[23] Chirnjeev Singh Nagi., Ogin, S.L., Iman Mohagheghian., Crean, C., Foreman, A. (2020). Spray deposition of graphene nano-platelets for modifying interleaves in carbon fibre reinforced polymer laminates, Materials and Design, 193, pp. 108831–108831. DOI: 10.1016/j.matdes.2020.108831.

[24] Zhou, H., Du, X., Liu, H.-Y., Zhou, H., Zhang, Y., Mai, Y.-W. (2017). Delamination toughening of carbon fiber/epoxy laminates by hierarchical carbon nanotube-short carbon fiber interleaves, Composites Science and Technology, 140, pp. 46–53. DOI: 10.1016/j.compscitech.2016.12.018.

[25] Quan, D., Farooq, U., Zhao, G., Dransfeld, C., Alderliesten, R. (2022). Recycled carbon fibre mats for interlayer toughening of carbon fibre/epoxy composites, Materials and Design, 218, p. 110671. DOI: 10.1016/j.matdes.2022.110671.

[26] Wong, D.W.Y., Zhang, H., Bilotti, E., Peijs, T. (2017). Interlaminar toughening of woven fabric carbon/epoxy composite laminates using hybrid aramid/phenoxy interleaves, Composites Part A: Applied Science and Manufacturing, 101, pp. 151–159. DOI: 10.1016/j.compositesa.2017.06.001.

[27] Vallack, N., Sampson, W.W. (2022). Materials systems for interleave toughening in polymer composites, Journal of Materials Science, 57(11), pp. 6129–6156. DOI: 10.1007/s10853-022-06988-1.

[28] Chen, Q., Wu, F., Jiang, Z., Zhang, H., Yuan, J., Xiang, Y., Liu, Y. (2023). Improved interlaminar fracture toughness of carbon fiber/epoxy composites by a combination of extrinsic and intrinsic multiscale toughening mechanisms, Composites Part B: Engineering, 252, p. 110503. DOI: 10.1016/j.compositesb.2023.110503.

[29] Xu, F., Yang, B., Feng, L., Huang, D., Xia, M. (2020). Improved Interlaminar Fracture Toughness and Electrical Conductivity of CFRPs with Non-Woven Carbon Tissue Interleaves Composed of Fibers with Different Lengths, Polymers, 12(4), p. 803. DOI: 10.3390/polym12040803.

[30] Beylergil, B., Tanoğlu, M., Aktaş, E. (2018). Effect of polyamide-6,6 (PA 66) nonwoven veils on the mechanical performance of carbon fiber/epoxy composites, Composite Structures, 194, pp. 21–35. DOI: 10.1016/j.compstruct.2018.03.097.

[31] Ou, Y., Wu, L., Yi, X., Mao, D. (2023). Understanding Mode I interlaminar toughening of unidirectional CFRP laminates interleaved with aligned ultrathin CNT fiber veils: Thickness and orientation effects, Composites Part B: Engineering, 254, pp. 110578–110578. DOI: 10.1016/j.compositesb.2023.110578.

[32] Cheng, C., Zhang, C., Zhou, J., Jiang, M., Sun, Z., Zhou, S., Liu, Y., Chen, Z., Xu, L., Zhang, H., Yu, M. (2019). Improving the interlaminar toughness of the carbon fiber/epoxy composites via interleaved with polyethersulfone porous films, Composites Science and Technology, 183, p. 107827. DOI: 10.1016/j.compscitech.2019.107827.

[33] Gheryani, A.A., Fleming, D.C., Reichard, R.P. (2019). Nonwoven polyester interleaving for toughness enhancement in composites, Journal of Composite Materials, 53(28-30), pp. 4349–4367. DOI: 10.1177/0021998319857116.

[34] Wang, S., Mehmet Çağatay Akbolat., Oğuzcan İnal., K.B. Katnam., Zou, Z., Potluri, P., Taylor, J. (2022). On the effect of binders on interlaminar fracture energies and R-curves of carbon/epoxy laminates with non-woven micro-fibre veils, Composites Part A: Applied Science and Manufacturing, 162, pp. 107150–107150. DOI: 10.1016/j.compositesa.2022.107150.

[35] Beckermann, G.W., Pickering, K.L. (2015). Mode I and Mode II interlaminar fracture toughness of composite laminates interleaved with electrospun nanofibre veils, Composites Part A: Applied Science and Manufacturing, 72, pp. 11–21. DOI: 10.1016/j.compositesa.2015.01.028.

[36] Ramji, A., Xu, Y., Yasaee, M., Grasso, M., Webb, P. (2020). Delamination migration in CFRP laminates under mode I loading, Composites Science and Technology, 190, p. 108067. DOI: 10.1016/j.compscitech.2020.108067.

[37] Restuccia, C.L. and Blackburn, R., Cytec Industries Inc, (2018). Hybrid veil as interlayer in composite materials. U.S. Patent Application 15/771, 532.

[38] ASTM D5528-13, Standard Test Method for Mode I Interlaminar Fracture Toughness of Unidirectional Fiber Reinforced Polymer Matrix Composites, ASTM International, West Conshohocken, PA, 2013.